

Automated Corrosion Identification in Metal Imagery: Traditional vs. Deep Learning

No Author Given

No Institute Given

Abstract. Microbial-induced corrosion (MIC) poses a significant challenge in various industrial settings, including space and ground flight applications. Identifying and mitigating corrosion in metallic surfaces is crucial for ensuring the structural integrity and longevity of engineering systems. Segmenting MIC allows for early detection and proactive repair, which improves safety and cost efficiency in environments such as the International Space Station. This study presents a novel baseline algorithm called CLF (clustering using local features) for MIC segmentation based on traditional Non-Deep Learning techniques. We compare our approach to two advanced Deep Learning models: DeepLabv3+ and the Segment Anything Model (SAM). The SAM model is experimented with for the first time in the context of MIC segmentation. Our results on a new MIC dataset of 154 images reveal that the SAM model excels, with an excellent Accuracy of 97.59% and a Dice Score of 71.36%. These promising outcomes highlight the potential of our methodologies and establish a strong foundation for future expansions upon the availability of further data. This research sets a critical path for further comprehensive studies in the field of MIC segmentation.

Keywords: Microbial-Induced Corrosion · Traditional baseline · Segment Anything Model · DeepLabv3+

1 Introduction and Motivation

Microbial-Induced Corrosion (MIC) of metal structures, containers, and pipelines represents a major global problem with an estimated economic loss of 2.5 trillion U.S. dollars [1]. Bacteria and other microorganisms associated with MIC typically grow as surface-adherent biofilm populations and, as such, are highly resistant to antimicrobial treatments. Biofilms are also associated with spacecraft and have been shown to cause fouling and corrosion with critical equipment related to life support, instrumentation, and structural components [2]. The water recovery system (WRS) on the International Space Station (ISS) is a crucial life support feature in that it collects waste liquids, including crew urine and breath humidity. It purifies the liquids via distillation and disinfection into safe potable water. Fig. 1 shows the biofilms that commonly occur in the bacteria-containing liquids prior to disinfection [3].

In order to assess biofilm growth and its potential role in MIC during spaceflight, the NASA Bacterial Adhesion and Corrosion (BAC) team [6] conducted

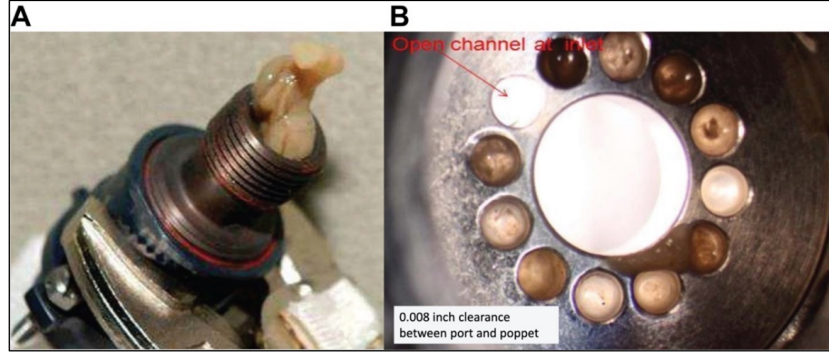


Fig. 1. International Space Station (ISS) Water Recovery System (WRS) components that needed to be replaced due to microbial-induced corrosion (MIC): (A) water condensate line and (B) on a solenoid valve [5].

two recent spaceflight studies that launched on Space X21 (2020) and Space X29 (2023). The team tested the ability of *Escherichia coli* and *Pseudomonas aeruginosa* ability to form biofilms and corrode stainless steel coupons in microgravity (spaceflight) and full-gravity conditions [6].

Scanning Electron Microscopy (SEM) is the standard method to get high-resolution images of biofilms for manual identification [7]. The McLean team [4] has already performed an SEM examination of the 316 Space X21 coupons and of the 316 ground coupons incubated under identical conditions, resulting in 9,415 SEM micrographs. In order to gain the most rigorous assessment of the scientific findings, it is necessary to obtain some quantitative data and analysis. Manual identification of corrosive damage is time-consuming and error-prone, highlighting the need for automated solutions that use advanced computer vision and machine-learning techniques.

Thus, this paper focuses on the initial results of collaboration between the Data Lab [9] and the Mclean team [4]. Here, we propose a novel approach for the SEM image analysis and provide quantitative answers for *any* future collection of samples on how Microbial-Induced Corrosion (MIC) is influenced by the presence or absence of the following factors: bacteria, chemical components, biological components, time of incubation, media composition, space or ground experiment, etc. [10]. We formulate the task as a computer vision task of semantic segmentation and focus on effectively segmenting MIC regions in SEM images against the non-MIC ones. This task can be effectively addressed using both traditional (Non-DL) and Deep Learning (DL) techniques. Non-DL methods, such as conventional image processing techniques, can offer more straightforward and faster solutions. These techniques, including thresholding, clustering, and graph-based algorithms, can improve efficiency and interpretability [13]. DL methods, such as DeepLab, Mask RCNN, and U-Net, are particularly effective for accurate and automated segmentation [14]. Both approaches have their advantages, with Non-DL methods being more interpretable and efficient, while DL methods offer higher accuracy and automation.

This paper is the first to consider the values of both approaches. It provides a benchmark for future MIC segmentation. We also propose a new tra-

ditional (Non-DL) approach. We adopt the two state-of-the-art DL methods, DeepLabv3+ and Segment Anything Model (SAM). SAM stands out as the top-performing model with the highest Dice Score of 71.36%.

2 Related Work

In [15], the researchers employed a self-supervised model called SimSiam architecture to detect Microbial-Induced Corrosion (MIC) in biofilm images. Their proposed approach leveraged a ResNet backbone and addressed similar challenges through image augmentations and overlapping patches. [7] summarizes a novel method for segmenting and quantifying bacterial cells in Scanning Electron Microscopy (SEM) biofilm images. The proposed method distinguishes and segments overlapping and touching cells more effectively than Mask R-CNN, as it includes the U-Net with ellipse fitting for semantic segmentation. [16] proposes an imaging system that makes use of SEM micro-graphs and OpenCV techniques. To detect bacterial aggregation, they utilized image contours and normalization for brightness and contrast adjustments. These methods provide reliable estimation of biofilm coverage, which aided in the evaluation of MIC on metallic surfaces. The study [17] uses DeepLabv3+ and Mask R-CNN models to automate the analysis of bacterial biofilm in microscopy images. Their AI-driven method significantly speeds up and enhances the accuracy of segmenting bacterial cells and measuring their properties, making it a promising alternative to traditional manual methods. In another study, [18] introduced a novel DL method that does not require per-pixel labeled data to segment images of rust corrosion on infrastructure effectively. The paper used Grad-CAM++, a DL classifier, to generate heat maps and Conditional Random Fields (CRF) to refine the segmentation masks. [19] presents HEU-Net, which combines Hybrid Attention Residual Blocks with External Skip Connections. This strategy improved corrosion detection accuracy. HEU-Net performed significantly better than previous models on the Metal Corrosion dataset. A U-Net architecture was used [20] to semantically segment corrosion in stereo microscope images of archaeological artifacts. This technique improved the efficiency and accuracy of corrosion detection and helped restorers with preservation. TransUNet was compared to UNet and DoubleUNet in [21] for microorganism segmentation in SEM images, highlighting TransUNet's superior performance due to its hybrid CNN and Vision Transformer architecture. This method offers improved accuracy for microbiological image analysis in bio-medicine. The three super-resolution techniques—ESRGAN, BSRGAN, and SwinIR—improved the segmentation result of biofilm images by enhancing the image quality and resolution [22]. The study [23] employed UAV imagery to detect and locate corrosion on steel structures. It used SLIC super-pixel segmentation in conjunction with Feature Pyramid Network (FPN) and Path Aggregation Network (PANet) for segmentation.

3 Methodology

In this section, we introduce our baseline for MIC segmentation using traditional Non-Deep Learning (Non-DL) methods thresholding and a novel algorithm combining clustering with local features. We also present two Deep Learning

(DL) models—DeepLabv3+ and Segment Anything Model (SAM)—as improved methods.

Traditional Non-DL Baseline: Non-DL methods, such as thresholding or clustering, provide a fast and straightforward approach to segmenting images based on simple criteria such as pixel intensity or spatial proximity. To apply this knowledge, we experimented with OpenCV’s [24] *threshold* method on our MIC dataset. This segmentation technique converts an image to a binary image by applying an intensity threshold, turning pixels with intensity above a specified threshold white and all others black. Since most of the corrosion regions in the pictures have high color intensity, this method helps to separate corrosion from the background.

In this research, we proposed an algorithm by combining traditional methods and named it *Clustering using Local Features (CLF)*. The algorithm starts with local feature detection [25] using keypoint extraction and description methods such as SIFT, ORB, or ORB with SIFT descriptors. Keypoints and descriptors help to capture distinctive features in an image for matching and recognizing objects across different views and scales. Following this, K-Means clustering is used to group similar descriptors to highlight key features and reduce complexity. Points are grouped spatially using DBSCAN clustering [26], which segments the image into coherent regions based on location and similarity. Subsequently, mask generation is applied to isolated segmented regions and refined using morphological operations to remove noise and fill gaps. Finally, contour processing refines these masks, focusing on specific sizes and shapes that improve the clarity of the segmentation. We have outlined all the process steps in the Algorithm 1.

Algorithm 1 Baseline Algorithm (CLF)

Require: Input image I

Ensure: Processed image

- 1: **Feature Detection:** Apply SIFT/ORB to detect key points and descriptors in images.
 - 2: **Descriptor Clustering:** Use KMeans to cluster descriptors.
 - 3: **Spatial Clustering:** Apply DBSCAN to key points based on their spatial location and feature similarity to segment coherent regions.
 - 4: **Mask Generation and Refinement:** Create and refine masks using morphological operations.
 - 5: **Contour Processing:** Extract and filter contours based on size and shape criteria.
 - 6: **Output:** Save or display processed images.
-

Deep Learning as an Improved Model: We implemented and fine-tuned two DL segmentation methods, DeepLabv3+ and SAM, to our MIC segmentation dataset. These DL methods have architectures that can learn complex patterns directly from the data, often yielding more accurate and robust results compared to traditional techniques. *DeepLabv3+* [27] is an advanced DL architecture for semantic image segmentation that has a robust encoder-decoder structure. It begins with an encoder that uses a backbone, such as ResNet [28] or Xception [29], to extract higher-level features from input images using pre-trained weights from large datasets like ImageNet. Additionally, the encoder uses different rates of atrous convolutions, often referred to as dilated convolution, which enables the

network to capture multi-scale contextual information without adding to the computational load. Increasing the feature map’s spatial resolution allows the decoder to refine segmentation outcomes, improving the boundary delineation of objects in the segmented image by integrating the low-level features with the high-level features via skip connections. DeepLabv3+ is flexible and robust and thus is suitable for precise segmentation tasks such as this one. The *Segment Anything Model (SAM)* [30] is a state-of-the-art method that uses prompt engineering to handle a variety of segmentation tasks. SAM is “promptable”, meaning that it can accept diverse types of inputs. This nature allows it to generate valid segmentation masks from many forms of prompts, such as points, boxes, or free-form text, making it highly flexible to different segmentation applications. It also allows SAM to perform tasks that require minimal prior training effectively. Three parts of the SAM architecture are a flexible prompt encoder that can handle various types of prompts, a Vision Transformer (ViT)-based image encoder that was pre-trained using Masked Auto-encoders (MAE), and a lightweight mask decoder that effectively creates segmentation masks by combining data from the image and prompt embeddings. SAM can adapt zero-shot to different tasks and data distributions; this allows it to achieve remarkable performance, frequently matching or surpassing that of fully supervised models [30].

4 Dataset Acquisition & Processing

4.1 Dataset

The team [4] performed a Scanning Electron Microscopy (SEM) examination of the 316 Space X21 coupons and the 316 ground coupons incubated under identical conditions. The coupons were mounted in a 12-well BioCell flight hardware [31]. The cultures for both Space X21 and Space X29 were prepared at Kennedy Space Center (Florida) immediately prior to flight and then inoculated during orbit by the space crew. Asynchronous ground controls were done at ASU several hours after the flight samples so that accurate reproduction of the experimentation could be performed following receipt of astronaut communications. The components were brought onto the International Space Station (ISS) aboard Space X21. At pre-selected times, some wells were inoculated by the ISS crew with a mixed bacteria culture. The same experiments and hardware were also conducted asynchronously by ground control.

After the flight and ground-control samples for SEM analysis were returned to the McLean team [4], they were processed first for confocal microscopy (which required intact BioCells). The team removed the stainless steel coupons from BioCell and chemically washed the biofilm coupons to prepare them for SEM imaging. The coupons were mounted onto SEM support stubs and then examined under vacuum at low magnification (50X) for a general scan and higher magnifications (typically 1,500X – 3,000X) that enabled bacteria and related corrosion to be observed. During SEM, energy is absorbed (from the electron beam), which then fluoresces in the X-ray spectrum, which is the energy characteristic of individual elements. There are several thousand SEM micrographs from the initial flight experiment (Space X21), and the samples were examined

with a JEOL SEM in both low and high vacuum settings [4]. The full dataset consists of 9415 TIFF images and associated metadata. The images vary widely depending on factors such as voltage, magnification, imaging method, resolution, etc. In order to establish an effective baseline, we focused on the most significant overlapping portions of our data, which narrowed our dataset to 4573 images. Of these, a domain expert labeled 154 images pixel-by-pixel (corrosion vs. background) to give us a ground truth (Fig. 2). Using Label Studio as the annotation software, we annotated in four batches, each batch contributing to the total. The dataset contains images and annotations for both corrosion and background only (132 corrosion to 22 background only). The corresponding 154 images and labels have resolutions of 1280×960 and 2560×1920 .

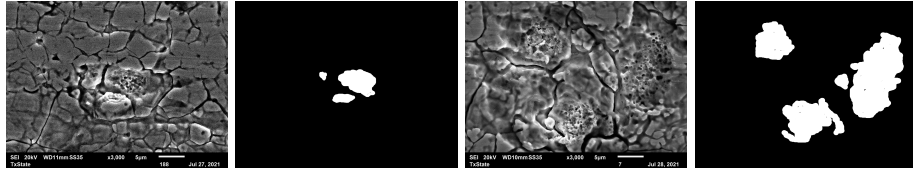


Fig. 2. Two sample images and their corresponding ground truth from our dataset.

4.2 Data Processing

Cropping: Textual information at the bottom of the images was cropped to ensure that both the DL and Non-DL methods process only relevant features, aligning the input data closer to the binary format of the ground truth.

Resizing: In the experiment, we used different variations of image sizes as required. In the proposed baseline experiments, we resize the images to 512x512 resolution. Also, when using images with higher dimensions, the segmentation gave noises and mostly incorrect results due to the dataset's complexity and high variability. Lowering the dimension to 512 helped the descriptors capture more relevant features and enhanced cluster separability, which led to better segmentation. In the experimented DL models, Deeplabv3+ utilized a resolution of 512x512 for both input images and their respective ground truths, and SAM utilized a resolution of 1024x1024 for input images and 256x256 for ground truths input.

Dataset Split: The dataset was split into train, validation, and test subsets with respective ratios of 65:15:20. These same splits were used with both DL models. We also applied k-fold cross-validation to SAM, using 50 epochs per fold to mitigate the issues of data leakage and over-fitting.

Data Augmentation: Because the number of corresponding images and annotations is small, augmentation techniques can help our DL models not to overfit. During training, we augmented the input images and annotations by applying the transformations: rotate, scale, jitter, flip, and affine.

Normalization: Pixel values across all images were normalized in the DL methods from a range of 0 to 1 to facilitate faster convergence during training.

Hyper-Parameters: *DeepLabv3+:* 8 batch size, the RMSprop optimizer, 0.001 learning rate, and 1e-3 weight decay; utilizing dice and binary-cross-entropy for the loss functions. *SAM:* 4 batch size, AdamW optimizer, 0.0001 learning rate,

and 1e-3 weight decay; utilizing DiceCELoss for the loss function. Both are trained using 100 epochs. SAM's training early stopping is after 15 epochs.

Evaluation Metrics: Non-DL: Dice Score, Intersection over Union (IoU), and Mean Squared Error (MSE) are used as they commonly quantify segmentation performance. DL: Accuracy, MCC, Precision, Recall, Dice Score, and IoU.

5 Experimental Results And Discussion

Table 1 summarizes the quantitative evaluation results of different applied approaches. **Traditional Non-DL Baseline:** All 154 images were utilized for the Non-DL baseline. The evaluation process compares the output masks to the corresponding annotated ground truth. The traditional *thresholding* approach was able to identify some regions of corrosion (Fig. 3). While it was able to identify areas, the predicted masks differ significantly from the ground truth, as captured by the Dice Score of 21.53% and an IoU of 13.06%. The challenge of segmenting MIC with thresholding is that the high levels of noise make it difficult to identify the boundaries of corroded regions clearly. We conclude that thresholding can provide critical preliminary insight but that it is insufficient for accurate automated corrosion identification.

The proposed algorithm *Clustering using Local Features (CLF)* shows a vast improvement over the thresholding method (Fig. 3). Among all the local feature methods combined with the CLF algorithm, SIFT gave the best Dice Score of 34.89% and IoU of 24.13%, indicating better overlap and segmentation accuracy. The Dice Score and IoU noticeably dropped by 8.69% and 5.15% without morphological operations in SIFT. SIFT without morphological operations showed the least MSE (4.2%), suggesting a minor improvement in pixel-wise accuracy compared to SIFT with morphological operations (4.61%). While CLF+ORB was more computationally efficient, it yielded a lower Dice Score (30.42%) and IoU (19.53%) than SIFT, indicating less accurate segmentation. Additionally, combining ORB keypoints and SIFT descriptors yielded the lowest Dice Score (25.50%) and IoU (16.50%), indicating poor segmentation accuracy. These findings emphasize the importance of using the appropriate feature descriptors and post-processing approaches to achieve effective segmentation in our proposed CLF algorithm. They also show how effective our proposed CLF algorithm is as a Non-DL technique for the MIC dataset.

Deep Learning as an Improved Model: The segmentation results using *DeepLabv3+* show both the strengths and limitations of the architecture and data. The model achieved a Dice Score of 69.53% and an IoU of 53.69%, indicating a reasonably good but not perfect overlap between the predicted and actual masks, as visualized in Fig. 5. The average Accuracy of 97.31% reflects a solid performance in the ability to distinguish between target areas and the background. The Recall of 67.57% suggests some challenges in capturing all actual positive areas, potentially missing finer details. The Precision of 69.04% confirms moderate exactness in predictions, implying occasional false positives and negatives. The MCC of 67.90% further suggests a good quality of binary classification. Overall, the model demonstrates robustness in general segmentation tasks. The next step is to expand the dataset size to better train the model.

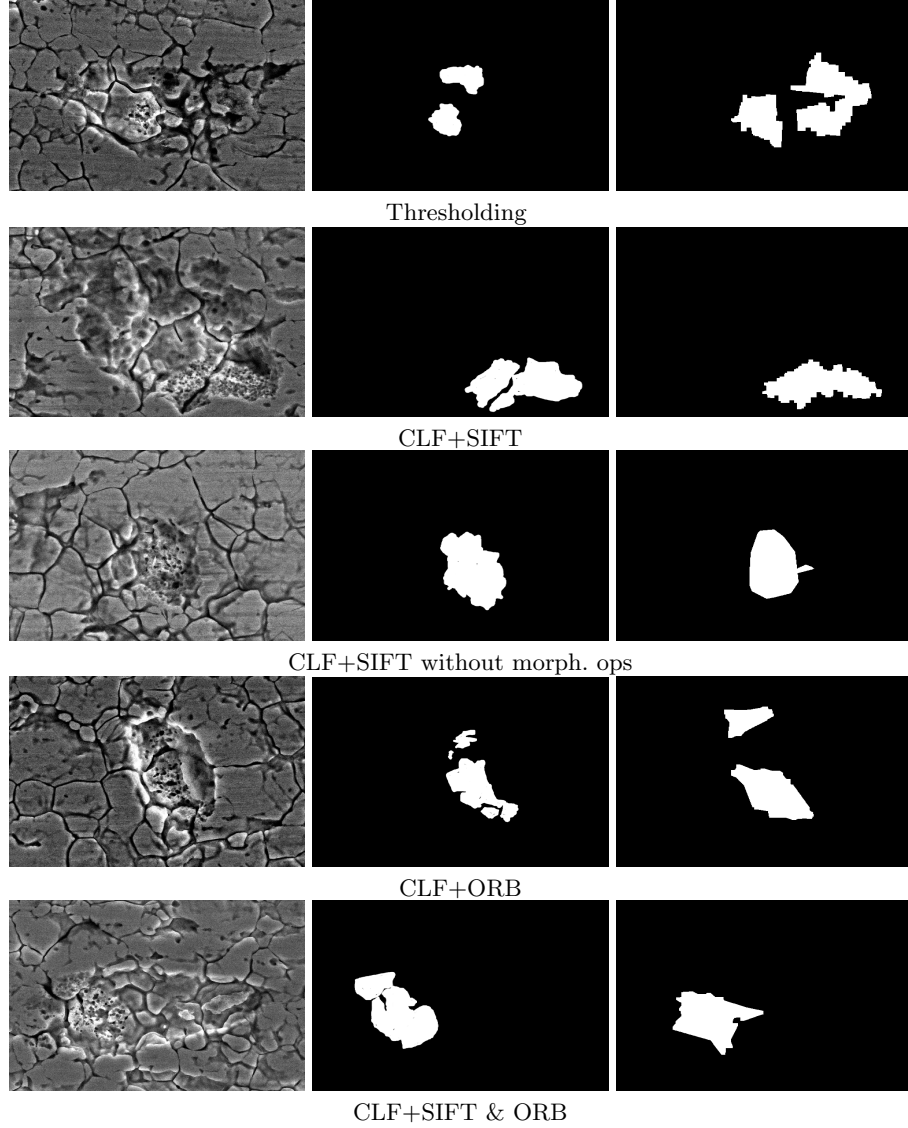


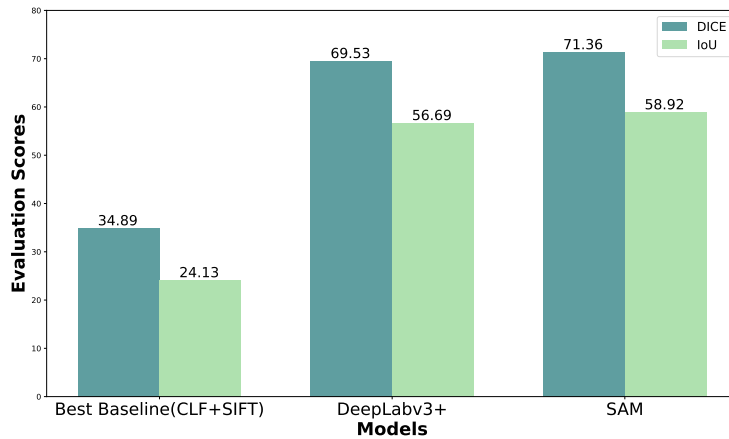
Fig. 3. Corrosion image (left), ground truth (middle) and predicted mask (right) utilizing traditional (Non-DL) techniques

The *Segment Anything Model* (SAM) results showcase its capabilities and limitations with the given small dataset. The average Dice Score of 71.36% and IoU of 58.92% indicate moderate success in capturing the relevant segmentation areas yet highlight room for improvement in precisely matching the ground truth, as evidenced by the segmented regions in the image plot. The high average Accuracy of 97.59% suggests that the model effectively identifies the background and significant areas well. With the primary focus being the regions of corrosion,

Table 1. Performance comparisons of implemented approaches on MIC dataset

Backbone	ACC%	MCC%	PRE%	RC%	Dice%	IoU%	MSE%
Thresholding	—	—	—	—	21.53	13.06	14.08
SIFT	—	—	—	—	34.89	24.13	4.61
SIFT (without morph. ops)	—	—	—	—	26.20	18.98	4.2
ORB	—	—	—	—	30.42	19.53	6.83
ORB & SIFT	—	—	—	—	25.50	16.50	5.43
DeepLabv3+	97.31	67.90	69.04	69.57	69.53	53.69	—
SAM	97.59	65.16	71.15	63.63	71.36	58.92	—
SAM (cross-validation)	97.68	67.29	72.79	66.63	70.25	58.05	—

the model's Recall is 63.63%, Precision is 71.15%, and MCC is 65.16%. These scores point to the model missing a third of corrosion pixels while labeling almost 30% of pixels falsely as corrosion. Overall, SAM demonstrates robust general segmentation ability for our MIC dataset but not great sensitivity and precision in segmenting intricate details, as illustrated in Fig. 5.

**Fig. 4.** Model performance comparison between CLF and DL models.

Performance Comparison: Fig. 4 compares and analyzes the performance of three different segmentation models using two metrics: Dice Score and Intersection over Union (IoU). The best baseline method using the proposed CLF algorithm (CLF+SIFT) performed the lowest on both Dice and IoU metrics, making it the least effective among the three approaches in terms of segmentation accuracy. In summary, the traditional Non-DL baseline techniques could not perform very well in identifying corrosion because of the variability of image characteristics like intensity, texture, etc. These techniques underperformed compared to supervised DL methods due to several fundamental limitations. The unsupervised methods do not use labeled data, which restricts their ability to segment images based on precise, predefined criteria. Also, they rely on fixed features that may not capture the complexities of the diverse local environment of SEM imagery. Thus, our traditional baseline achieved a Dice Score of 34.89%.

The DL approaches performed notably better than the Non-DL methods. DeepLabv3+ showed a significant improvement over the best Non-DL baseline, nearly doubling the Dice Score and IoU. DeepLabv3+ was the second-best-

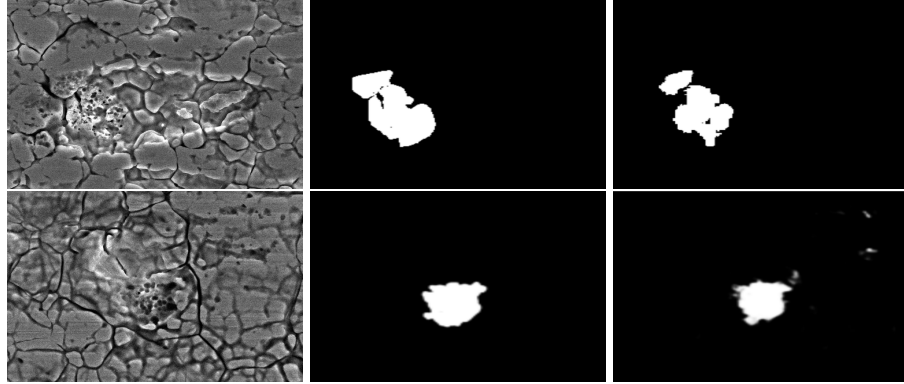


Fig. 5. Corrosion image (left), ground truth (middle), and predicted mask (right) utilizing SAM model (top) and DeepLabv3+ model (bottom)

performing method, indicating a robust capability for segmentation tasks. SAM showed notable improvements in several metrics compared to DeepLabv3+. The Accuracy improved by 0.28%, and the Precision showed a 2.11% increase, which was even further increased by 3.75% with the utilization of cross-validation. While DeepLabv3+ had a 5.94% higher recall than SAM, the Dice Score of SAM showed a 1.83% improvement. The SAM model's reduction in false positives ensured a higher improvement in the IoU compared to the Dice Score, which is less sensitive to changes in false positives and false negatives. We have achieved the most significant improvement with a 5.23% IoU increase in the SAM model over DeepLabv3+.

6 Conclusion & Future Work

Microbial-Induced Corrosion (MIC) damages metal surfaces, and this damage has the potential to be automatically detected using different techniques. This unique collaboration between the state-of-the-art computer science analytical approaches and a microbiology group dramatically enhances the caliber of the scientific effort, as it promotes the safety of future spaceflight beyond low Earth orbit. We developed techniques for segmenting corrosive regions that utilized both traditional Non-DL and DL methods: We applied thresholding—a traditional Non-DL approach—, we developed CLF—a new Non-DL algorithm tailored for MIC segmentation, and we implemented two advanced DL models—DeepLabv3+ and SAM. Utilizing CLF, we established a robust baseline, achieving a 34.89% Dice Score without relying on annotations. Enhancing our DL models, we showed significant improvement, with SAM achieving the best result at a 71.36% Dice Score. The MIC dataset only consists of 154 annotations from thousands of Space X21 images due to the inconsistent data gathering procedures and lack of annotations. This is one of the limitations to getting a reasonable but not very efficient performance, as DL models require a large amount of data to learn and generalize features. We are also streamlining the image capture of the Space X29 coupons to help us simplify data capture and the annotation process. For the annotation, we plan to use energy-dispersive X-ray (EDX) imagery as the baseline for the semi-supervised corrosion annotation. EDX captures the

elemental composition in a specimen, and oxygen and iron can pinpoint the corrosion location [32].

Acknowledgments. This work has been partially supported by the NSF # 2224449 grant, the NASA # 80NSSC22K1361 grant, and the Texas State University Research Enhancement Program grant.

References

1. Procópio, L.: Microbially induced corrosion impacts on the oil industry. In: *Archives of Microbiology*. **2024**(2), p. 138. Springer (2022).
2. Yang, J., et al.: Microbiology of the built environment in spacecraft used for human flight. In: *Methods in Microbiology*. **45**, pp. 3-26. Elsevier (2018).
3. Zea, L., et al.: Potential biofilm control strategies for extended spaceflight missions. In: *Biofilm*, **2**, p. 100026. Elsevier(2020).
4. McLean, R.J.C.: Microbiology of Biofilms and Polymicrobial Communities. <https://mcleanlab.wp.txstate.edu/dr-mclean> (2024).
5. Carter, D.L. and Brown, C.: Impact of biofilms on the design and operation of ISS life support systems. In: Annual meeting of the American Society for Gravitational and Space Research (ASGR 2017). no. M17-6276 (2017).
6. NASA Ames Research Center: Bacterial Adhesion and Corrosion (SpaceX-21). <https://www.nasa.gov/ames/space-biosciences/bacterial-adhesion-and-corrosion-spacex-21/> (2021).
7. Abeyrathna, D., et al.: Segmentation of bacterial cells in biofilms using an overlapped ellipse fitting technique. In: 2021 IEEE International Conference on Bioinformatics and Biomedicine (BIBM). pp. 3548-3554. IEEE (2021).
8. Yang, J., et al.: Microbiology of the built environment in spacecraft used for human flight. In: *Methods in Microbiology*. Academic Press. **45**, pp. 3-26. Elsevier (2018).
9. Tešić, J.: Data Lab. <https://datalab12.github.io> (2024).
10. Knisz, J., et al.: Microbiologically influenced corrosion—more than just microorganisms. In: *FEMS microbiology reviews*. **47**(5), p. fuad041. Oxford University Press (2023).
11. Obenhuber, D.C., Huff, T.L. and Rodgers, E.B., 1991.: Microbial biofilm studies of the environmental control and life support system water recovery test for space station freedom. In: *SAE transactions*. pp. 888-892. JSTOR (1991).
12. Relucenti, M., et al.: Microscopy Methods for Biofilm Imaging: Focus on SEM and VP-SEM Pros and Cons. In: *Biology*. **10**(1), p. 51. MDPI (2021).
13. Mubashshira, S., Azam, M.M. and Ahsan, S.M.M.: An unsupervised approach for road surface crack detection. In: 2020 IEEE Region 10 Symposium (TENSYMP). pp. 1596–1599. IEEE (2020).
14. Minaee, S., et al. Image segmentation using deep learning: A survey. In: *IEEE transactions on pattern analysis and machine intelligence*. **44**(7), pp.3523-3542. IEEE (2021).
15. Bommanapally, V. et al.: Self-supervised learning approach to detect corrosion products in biofilm images. In: 2021 IEEE International Conference on Bioinformatics and Biomedicine (BIBM). pp. 3555-3561. IEEE (2021).
16. Iannucci, L., et al.: An imaging system for microbial corrosion analysis. In: 2019 IEEE International Instrumentation and Measurement Technology Conference (I2MTC). pp. 1-6. IEEE (2019).

17. Ragi, S., et al.: Artificial Intelligence-Driven Image Analysis of Bacterial Cells and Biofilms. In: IEEE/ACM Transactions on Computational Biology and Bioinformatics. **20**(1), pp. 174-184. IEEE (2023).
18. Burton, B., Nash, W.T. and Birbilis, N.: RustSEG—Automated segmentation of corrosion using deep learning. arXiv preprint arXiv:2205.05426 (2022).
19. Zhu, T., et al.: HEU-Net: hybrid attention residual block-based network with external skip connections for metal corrosion semantic segmentation. In: The Visual Computer, vol. **40**(2), pp. 1273-1287. Springer (2024).
20. Stocean, R., et al.: Semantic Segmentation for Corrosion Detection in Archaeological artifacts before Restoration. In: 2021 23rd International Symposium on Symbolic and Numeric Algorithms for Scientific Computing (SYNASC). pp. 246-251. IEEE (2021).
21. Gurung, B. D. S., et al.: Transformer in Microbial Image Analysis: A Comparative Exploration of TransUNet, UNet, and DoubleUNet for SEM Image Segmentation. In: 2023 IEEE International Conference on Bioinformatics and Biomedicine (BIBM). pp. 4500-4502. IEEE (2023).
22. Ashaduzzman, M., et al.: Using Deep Learning Super-Resolution for Improved Segmentation of SEM Biofilm Images. In: 2022 IEEE International Conference on Bioinformatics and Biomedicine (BIBM). pp. 3587-3593, IEEE (2022).
23. Han, Q., Zhao, N. and Xu, J.: Recognition and location of steel structure surface corrosion based on unmanned aerial vehicle images. In: Journal of Civil Structural Health Monitoring. **11**(5), pp. 1375-1392. Springer(2021).
24. Bradski, G.: The OpenCV library. In: Dr. Dobb's Journal: Software Tools for the Professional Programmer. **25**(11), pp. 120-123. Miller Freeman Inc. (2000).
25. Smelyakov, K., et al.: Local feature detector performance analysis on the digital image. In: 2019 IEEE International Scientific-Practical Conference Problems of Infocommunications, Science and Technology (PIC S&T). pp. 644–648. IEEE (2019).
26. Khan, K., et al. DBSCAN: Past, present, and future. In: The fifth international conference on the applications of digital information and web technologies (ICADIWT 2014). pp. 232-238. IEEE (2014).
27. Chen, L. C. et al.: Encoder-decoder with atrous separable convolution for semantic image segmentation. In: Proceedings of the European conference on computer vision (ECCV). pp. 801-818 (2018).
28. Koonce, B. and Koonce, B.: ResNet 50. In: Convolutional Neural Networks with Swift for Tensorflow. pp. 63-72. Springer (2021).
29. Chollet, F.: Xception: Deep learning with depthwise separable convolutions. In: Proceedings of the IEEE conference on computer vision and pattern recognition. pp. 1251-1258 (2017).
30. Kirillov, A., et al.: Segment anything. In: Proceedings of the IEEE/CVF International Conference on Computer Vision. pp. 4015-4026 (2023).
31. University of Colorado Boulder: BioServe Space Technologies: BioCell. <https://www.colorado.edu/center/bioserve/spaceflight-hardware/biocell> (2024)
32. Goldstein, J. I., et al.: Scanning electron microscopy and X-ray microanalysis. Springer (2017).